Bench-scale Microfluidic Manufacturing of Cross-linked Polyester Microparticles

AUTHOR NAMES: J. R. Bufton[1]*, D. C. Burns[2], J. Watchorn[3,4], Seoyeon Lee[1], C. Allen[1,3,4]*

AUTHOR ADDRESS:
1. Leslie Dan Faculty of Pharmacy, University of Toronto, Toronto, M5S 3M2
2. CSICOMP NMR Facility, Department of Chemistry, University of Toronto, Toronto, ON, M5S 3H6, Canada
3. Department of Chemical Engineering & Applied Chemistry, University of Toronto, Toronto, ON, M5S 3E5, Canada
4. Acceleration Consortium, Toronto, ON, M5S 3H6, Canada

KEYWORDS: Long-acting therapeutics, Microspheres, Advanced continuous manufacturing, Drug delivery, Polymer materials

ABSTRACT
Polymeric microparticles used as long-acting drug delivery systems provide advantages relative to conventional oral dosage forms including improved efficacy and safety. However, development of these formulations, including generics, is constrained by current manufacturing techniques. Conventional approaches have limited control over process parameters and are difficult to scale. Droplet microfluidic techniques produce individual particles sequentially enabling unparalleled consistency on key material properties including particle size and dispersity. While microfluidics approaches have much promise, including affording continuous rather than batch production; designing, constructing, and operating these systems is challenging reducing adoption by formulation scientists. Herein, we describe the operation of a modular microfluidic system built with commercially available components to prepare photo-cross-linked microparticles by droplet generation, inline dilution, and inline irradiation with UV. We synthesized monodisperse cross-linked polyester microparticles with a median size of 37.6 ± 0.4 µm at 20, 60 and 120 mg batch sizes with average yields of 92 ± 5 %. Additionally, as a means to tailor material properties, particles were produced at varying degrees of cross-linking. The particle's properties were further characterized, loaded with celecoxib at a low and a high level, then the *in vitro* drug release evaluated. Overall, the degree of cross-linking and drug loading modulated key formulation properties such as *in vitro* release rate. With this work, we showcase the potential of microfluidic systems and aim to foster further adoption of microfluidic techniques to manufacture comparable materials.

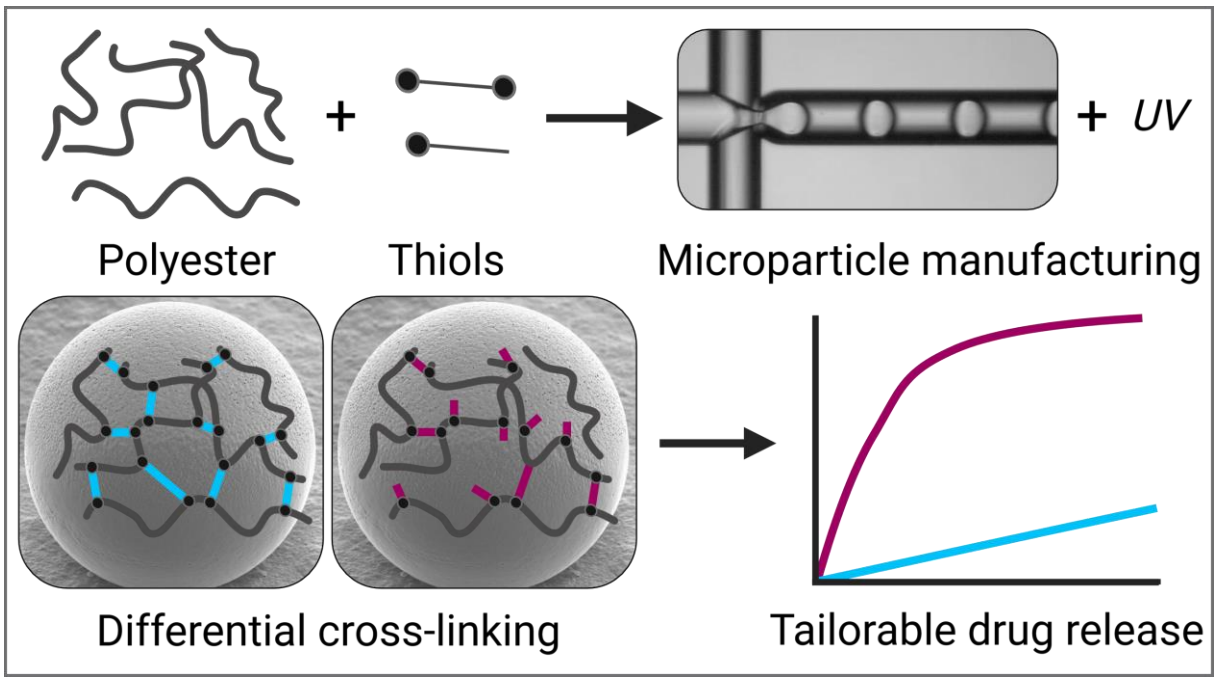

1. INTRODUCTION

With a globally aging population, the development of technologies to treat chronic disease is an increasing priority [1]. Aside from implants and *in situ* forming gels, polymer-based microparticles (MPs) are a popular strategy to prepare long-acting injectables (LAIs) [2,3]. These are micron-sized biodegradable particles that encapsulate a drug and provide sustained parenteral drug release [4,5]. In these systems, drug release is enabled via various mechanisms including diffusion, erosion, and swelling [6]. LAI formulations can confer several advantages over conventional oral dosage forms including improved patient adherence, lower medication burden, reduced first-pass metabolism, and sustained drug levels that can lead to a more consistent therapeutic effect with fewer side effects [7–9].

The first MP formulation, Lupron Depot®, was approved by the FDA in 1989 for delivery of a synthetic peptide to palliatively treat prostate cancer and then subsequently to treat central precocious puberty and endometriosis in 1993 and 2012, respectively [10,11]. Nowadays, there are a number of clinically-approved MP-based LAIs for treatment of a wide range of indications with many more in development [12–14]. To date, the vast majority of FDA-approved polymer MPs are composed of poly(lactide-*co*-glycolide) (PLGA) due to its biocompatibility and good safety profile. The composition of PLGA including the lactide to glycolide ratio, molecular weight, and end group chemistry as well as manufacturing processing parameters can be varied to tailor the physicochemical properties of the drug-loaded MPs and drug release rate [2]. To expand the material alternatives to PLGA, MPs have been prepared from poly(caprolactone) [15], methacrylates [16], hydrogels [17], naturally-sourced polymers [18], and silica [19]. Our group has explored polyesters functionalized with pendant olefinic groups which can be UV irradiated to prepare cross-linked polyester MPs (xMP) [20,21].

In spite of much academic work, clinical translation of MPs remains limited in part due to complex manufacturing processes. The majority of clinically approved MPs are manufactured in batches by coacervation, bulk emulsification or spray-drying [22]. These techniques have limited control over MP size, and difficulties achieving high yields as well as consistency across batches [12,23]. A multitude of material (e.g., polymer composition) and process parameters (e.g., equipment geometry) collectively determine the properties of the MPs which hinder technology transfer, scale-up, and post-approval process changes [22]. For example, Nutropin Depot® the only FDA approved protein-loaded MP was withdrawn from the market in 2004 because of complications encountered in scaling up production; preparing a single 500-gram batch required two weeks [24,25]. The manufacturing complexity also contributes to the lack of generic MP-based LAI products being approved despite the expiry of patent protection for reference listed drugs [14]. As a result, alternative manufacturing techniques have been explored [26].

In the last 20 years, microfluidic methods have been increasingly deployed pre-clinically to produce polyester [27–50] and cross-linked [23,51] MPs. The simplest manufacturing technique, emulsification, generates polymer droplets by applying shear to two immiscible fluids and then removing the dispersed phase solvent (typically by extraction or evaporation) to yield MPs [22]. In contrast, microfluidic techniques produce droplets sequentially introducing immiscible fluids at a microchannel junction, rather than all at once. Particles produced with microfluidic have shown higher monodispersity, encapsulation efficiency, and yields compared to bulk emulsification or spray-drying [33]. Additionally, microfluidic has the potential to be incorporated into continuous manufacturing processes affording greater flexibility and reduced scale-up difficulties compared to batch techniques [52–54]. However, the small characteristic length (i.e., >1 mm) of microfluidic-based droplet generation necessitates more stringent manufacturing conditions in terms of specialized equipment and training compared to conventional techniques, discouraging widespread adoption. Recent publications have highlighted the need to consider the microfluidic system components as a whole rather than a sole focus on the microfluidic chip to achieve reliable operation [35].

In this study, we describe the design and operation of a microfluidic system, reliant on commercially available components, to produce xMP. We prepared particles, denoted 1xMP, using the pendant functionalized polyester poly(1-allyl-3-methyl-glycolide) (*p*PLA) and hexanedithiol (HDT). Nominal batch sizes of 1xMP were prepared from 20–120 mg at 60 mg/hr achieving 92 ± 5 % yields. Furthermore, various stoichiometric mixtures of both HDT and propanethiol (PT) were reacted with pPLA to produce particles with nominal degrees of cross-linking of 0.75 and 0.5 (denoted 0.75xMP and 0.5xMP, respectively) with distinct material properties. The xMP were characterized, loaded with the drug celecoxib (CXB) at low and high levels, and the release was evaluated *in vitro*.

2. MATERIALS & EQUIPMENT

2.1 Reagents

Methanol (MeOH) and Dichloromethane (DCM) were purchased from Caledon Laboratory Chemicals. Poly(vinyl alcohol) (PVA [Mw 13–23 kDa]), deuterated dimethyl sulfoxide (DMSO-d6), tetrahydrofuran (THF), ethyl acetate (EA), 2,2-dimethoxy-2-phenylacetophenone (DMPA, 99%), acetone, 1,6-hexanedithiol (HDT, 96%) 1-propanethiol (PT, 99%), trifluoroacetic acid (TFA), phosphate buffered saline (PBS), sodium dodecyl sulfate (SDS), were purchased from

Sigma-Aldrich. Poly(1-allyl-3-methyl-glycolide) (AI108) (*p*PLA) was purchased from Akina (Indianapolis, USA). Celecoxib (CXB) was purchased from Toronto Research Chemicals (Toronto).

2.2 Microfluidic Equipment

A 3D flow-focusing droplet generator with hydrophilic channels (Dolomite 3200433); droplet generation chip hydrophilic channels (Dolomite 3000436); pressure pumps (Dolomite Mitos 3200175); oil-free air compressor (California Air Tools); flow sensor (30–1000 µL/min) (Dolomite Mitos 3200097); flow sensor (1–50 µL/min) (Dolomite Mitos 3200098) with a converter (Dolomite 3200285); chip H interface (Dolomite 3000155); 4-way linear connector (Dolomite 3000024); 1/4 in.-28 flangeless fittings (IDEX, XP-230); 1/4 in.-28 super flangeless fittings (IDEX, XP-141); 1/4 in.-28 straight female couplings (Dolomite 30000399); ethylene tetrafluoroethylene (ETFE) 1/4-28 female to female luer, (IDEX, P-678); fluorinated ethylene propylene (FEP) tubing with 0.1 mm, 0.25 mm, and 0.5 mm inner diameters (Dolomite 3200300, 3200063, 3200064, respectively); linear connector 4-way (Dolomite 3000024); ferrule with integrated filter (Dolomite 3200245); PEEK-Sil flow resistors (Dolomite 3200269, 3200271) sensor interface (Dolomite 3200200); end fittings and ferrules for 1.6 mm tubing (Dolomite 30000477); 2-way in-line valve (Dolomite 3200087); digital high-speed microscope (Dolomite 3200531); X-Y stage for high-speed digital microscope (Dolomite 3200600); flow-control center software (Dolomite 4.1.9 free version); 6-way rotary valve (e.g., IDEX CV900-100); and a UV curing oven (UVP 95-0228-01).

2.3 Cross-linked Microparticle Characterization

Following synthesis, xMP were characterized with a variety of techniques including light microscopy, laser light scattering, scanning electron microscopy, infrared spectroscopy, nuclear magnetic resonance and differential scanning calorimetry. Subsequently, xMP were loaded with CXB at 5 and 40 wt% initial drug-to-material ratios via immersion in a common organic solvent. The loading efficiency, morphology and thermal properties of CXB loaded xMP were also characterized. Finally, the *in vitro* release kinetics were assessed using the sample-and-separate method. Full details are given in section 2 of supporting information.

3. MICROFLUIDIC MANUFACTURING

3.1 System Overview

In previous work, we prepared xMP using standard bulk emulsification and then irradiated the emulsion with UV light [19]. In this contribution, xMP were synthesized by integrating the established bulk emulsion technique microfluidic flow-focusing for droplet formation [30]. The microfluidic system described herein is pressure-driven and produces reactive *p*PLA droplets via 3D flow-focusing. These droplets are subsequently diluted in a secondary flow-focusing chip (**Fig. 1a**) and then UV-irradiated inline (UV oven, $\lambda_{irradiation}$ 365 nm, 100 µJ/cm^2, 3.5 minutes) to facilitate thiol-ene cross-linking (**Supplementary Video 1**). In section 3 of supporting information, we provide additional detail, discussion and practical tips to help interested readers deploy microfluidic techniques for comparable applications. We also recommend the following publications to provide background to those unfamiliar with: building MF systems [35,55], MF droplet generation mechanics [56,57], and MF cross-linking [23,51].

During xMP production, five distinct fluids were used, each serving a specific purpose: 1) sample indicator (DCM with orange pigment), 2) sample (reactive *p*PLA solution), 3) sample driver

(DCM), 4) surfactant (PVA solution), and 5) diluent (PVA solution with NaCl). The complete compositions and functions of the fluids are detailed in **Fig. 1b** (further details on fluid preparation are given in section 3.7 of supporting information).

The microfluidic system was configured as illustrated in **Fig. 1a**. To ensure solvent compatibility, fluidic fittings were composed of FEP, ETFE, poly(tetrafluoroethylene) (PTFE), poly(ether-ether ketone) (PEEK), stainless steel or glass. The microfluidic system is pressure-driven with pumps (Dolomite Mitos 3200175) that have a 30 mL capacity and operate up to 10 bar. Five accompanying thermal mass flow sensors (Dolomite Mitos 320096-3200100) provide access to a wide range of flow rates (i.e., 70 nL/min to 5 mL/min). Some of the advantages of pressure pumps compared to syringe pumps (e.g., pulseless-flow, low response time) have been described elsewhere [35,58–60]. While using syringe pumps is feasible for producing xMP, we highlight the ease of switching fluids (simply replacing the vial in the pressure vessel) and real-time flow rate/pressure monitoring as features that increase the practicability of operation and troubleshooting using pressure pumps.

Due to its reasonable transmission at 365 nm, FEP tubing was used in the UV oven [61]. Fluid lines B and C (**Fig. 1a**) have inline filters (2 µm, stainless steel) which are a redundant risk-reduction measure to ensure particulates do not reach the primary chip. To clean fouled/clogged chips, a dedicated chip cleaning rig was employed (**Fig. 1a**). Wherein aqueous fluid lines were split for flow focusing, microfluidic T-junctions (**Fig. 1a**) were used in lieu of larger void volume PEEK T-junctions to reduce bubble formation. Moreover, flow resistors were incorporated downstream of the microfluidic chips to reduce bubble formation. The backpressure regulators placed downstream of detectors in some HPLC systems have an identical function [62]. Flow resistors were also placed upstream of microfluidic chips to stabilize flow rates. Despite using pressure-pumps (which are pulseless) upstream flow resistors were required to dampen oscillations caused by the mixing of immiscible fluids as well as other components in the described system (e.g., inline filters, hydrodynamic compliance of FEB tubing).

The physicochemical properties of the sample fluid (i.e., reactive *p*PLA solution) make it challenging to manipulate within microfluidic geometries using pressure pumps. The sample fluid is viscous, viscoelastic, volatile, light-sensitive, and fetid (due to the thiol cross-linker). Therefore, taking inspiration from common HPLC systems, a 6-way rotary valve with a sample loop was used and sample driver fluid (i.e., DCM) was placed in the pressure pump chamber. In addition to avoiding sample fluid evaporation in the pressure pumps, advantages to using driver fluids include: 1) reduction in waste as the dead volume between the primary chip and the sample fluid is decreased (i.e., it doesn't pass through the flow sensor), 2) lower pressure required to achieve a given flow rate due to the lower viscosity of the sample driver fluid, DCM, than the reactive *p*PLA solution, 3) cleaning of the system by the sample driver fluid once it has pushed the sample through the loop. The length of the sample loop was adjusted to alter the batch size of MPs being manufactured. In the current study, 200, 600, and 1200 µL sample loops (with tubing I.D. <1 mm) were used to produce 20, 60, and 120 mg batches of 1xMP (0.75xMP and 0.5xMP were only produced at 120 mg batch sizes).

3.2 Procedure

First, the microfluidic system was conditioned with sample driver, surfactant and diluent fluids (see section 3.8 in supporting information for additional detail). To load the sample loop, a dedicated pressure pump was used (pump A, **Fig. 1a**) and the sample indicator fluid was first

pumped through so that loading could be determined visually (i.e., the fluid displaced into the sample waste turned from orange to colorless) (**Fig. S1a**). The sample was kept pressurized (1600 mbar) using the 2-way valves on either side of the sample loop. Pressurizing the sample minimized flow rate disruption when the sample loop was introduced into the flow path.

The primary microfluidic chip is designed to create droplets from 25–70 µm in diameter. The 3D pore geometry prevents the sample fluid wetting the channel walls at the junction reducing fouling [56,63,64]. The flow rates of the sample driver and surfactant fluids (10 and 35 µL/min, respectively) were chosen as they resulted in dripping droplets [55].

Thiol-ene reactions occur on the order of seconds to minutes [65]. Accordingly, we selected a UV exposure time of 3.5 minutes. Inline dilution was incorporated in a secondary microfluidic chip to mitigate clogging. The diluent flow rate was 135 µL/min which corresponds to a 4-fold dilution of the primary chip outlet (180 µL/min total flow rate). During preliminary studies, we found the cross-linking tubing still clogged over longer periods of operation when using DI as the diluent (i.e., after 30 minutes). The composition of the dilution fluid was changed to 1wt% PVA and clogging was no longer observed. However, we found that the resulting xMPs had a subpopulation of much smaller particles despite the high homogeneity of droplets being produced in the primary chip (**Fig. S2**). We hypothesized that the loss in homogeneity arose from droplet fission that was occurring in the cross-linking tubing. Therefore, increasing the ionic strength of the diluent would increase the interfacial surface tension and reduce droplet fission [66]. Adding 4wt% NaCl to the diluent was found to be sufficient to maintain the homogeneity of the xMPs (**Fig. S2**). As a result, the composition of the diluent fluid was optimized to 1wt% PVA + 4wt% NaCl.

Following the completion of a microfluidic run, the xMPs were worked up as previously described by our group [20]. In brief, they were washed three times in DI, then acetone, and again with DI (centrifuging each time to remove the supernatant) before being lyophilized.

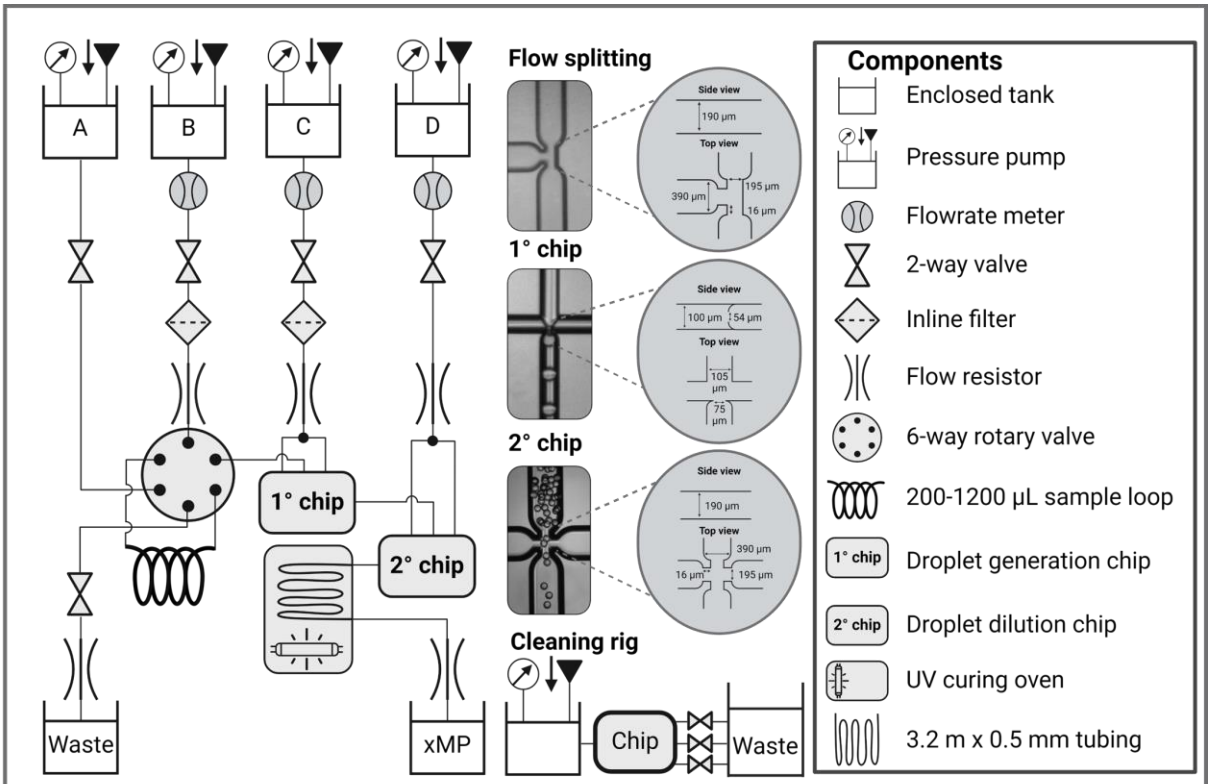

b

Name	Function	Solute	Solvent
Sample indicator	Shows the operator when the sample loop has been filled with sample	2-5wt% of turmeric + chili powder	DCM
Sample	Reactive polymer solution to prepare cross-linked microparticles	1) 7.5% (w/v) *p*PLA, 2) 0.5 allyl-molar equivalents DMPA 3) 0.5 or 0.38 or 0.25 allyl-molar equivalents HDT 4) 0 or 0.25 or 0.5 allyl-molar equivalents PT	DCM
Sample driver	Pushes the sample fluid through the MF system	-	DCM
Surfactant	Stabilizes droplets formed in the primary MF chip	2wt% PVA	Water
Diluent	1) Increases velocity of the droplets to avoid sedimentation and clogging during cross-linking 2) Reduces droplet fission during cross-linking	1wt% PVA + 4wt% NaCl	Water

c

Stage of operation	Fluid in pressure pumps						
	DI	IPA	Sample driver	Sample indicator	Sample	Surfactant	Diluent
Storage	C, D	A, B	-	-	-	-	-
Bubble removal	C, D	-	A, B	-	-	-	-
Conditioning	-	-	B	A	-	C	D
xMP production	-	-	B	-	A	C	D

Figure 1. a Schematic of the pressure-driven (Dolomite Mitos 3200175) microfluidic system configuration used in the current studies to produce cross-linked microparticles (xMP) with microfluidic junction geometries and cleaning rig. **b** Function and compositions of the fluids used to prepare cross-linked microparticles by microfluidics. **c** Tabulated fluids placed in the pressure pumps during storage, to remove bubbles, to condition, and to run samples. Abbreviations: microfluidic (MF), isopropyl alcohol (IPA), deionized water (DI), poly(1-allyl-3-methyl-glycolide)

(*p*PLA), 2,2-dimethoxy-2-phenylacetophenone (DMPA), 1,6-hexanedithiol (HDT), propanethiol (PT), poly(vinyl alcohol) (PVA), dichloromethane (DCM).

4. RESULTS & DISCUSSION

4.1 Droplet Size, Batch Yield & Particle Size

The initial size of the 1xMP droplets was assessed over the course of the run (i.e., during the first, second, and last third) by taking images of the droplets generated for all batch sizes (20, 60, or 120 mg). The runtimes varied from 20–120 minutes. Overall, the average size of the 1xMP droplets from all batch sizes across the duration of the run was 69.5 ± 3.2 µm (**Fig. 2a**). The average droplet size of 0.75xMP and 0.5xMP were similar (69.1 ± 3.6 and 68.9 ± 1.7 µm, respectively). Over a 120-minute run, the recorded flow rates were stable and within 10% of the target (**Fig. S1b**) and no fouling or clogging was observed. The flow sensors accuracy, determined gravimetrically, was 21.6 1.3, 3.1 ± 0.78, and 16.6 ± 1.7 % for the sample driver, surfactant and diluent fluids, respectively (**Fig. S1c**). The accuracy of the flow sensors (i.e., percent difference between measured and target flow rates) was proportional to the relative difference in specific heat and density between the operating fluid and the fluid to which the flow sensor was calibrated (hexadecane and water for organic and aqueous lines, respectively) (**Fig. S1c**). In future studies, calibration curves can address the discrepancy between the target and actual flow rates.

The average batch yield for 1xMP was 92 ± 5 % (**Fig. 2b**). Higher yields (98 ± 3 %) were achieved with the 120 mg batch. The yields for 0.75xMP and 0.5xMP (120 mg batch only) were slightly lower at 93.9 ± 10.2 and 81.9 ± 12.8, respectively. To ensure residual water did not confound the reported yields, we lyophilized one batch of 0.5xMP, 0.75xMP and 1xMP overnight, then weighed the vials, and then lyophilized for a further 24 hours. We found the weight changed by less than 1% (data not shown). To the author's knowledge, only one other publication preparing polymeric MPs via microfluidic has reported the batch yield (73–76%) [33]. Having an adjustable batch size has some considerable advantages during formulation development. With a smaller amount of xMP (i.e., 20 mg), various manufacturing parameters (e.g., flow rates, polymer concentration etc.) can be explored and optimized while reducing material and time. When more material is required for xMP characterization, the batch size can be increased simply by including a larger sample loop in the microfluidic system. In the current study we used 200–1200 µL sample loops as a proof of concept; there are no technical limitations to further increasing or reducing this.

Following cross-linking, xMPs were washed three times in aqueous and organic solvent to remove PVA, DCM, and residual thiols before lyophilization. The particle size distribution was assessed using laser light scattering (Mastersizer 3000, Malvern) (**Fig. 2c, d**). The median size of 1xMP was 37.6 ± 0.4 µm. The SPAN (0.4 ± 0.02) is a measure of the interdecile range of particle sizes normalized by the median and indicates that the MPs have a narrow size distribution. Both 0.75xMP and 0.5xMP had a similar particle size distribution of 1xMP, though there was a slight trend of increasing polydispersity with decreasing cross-linking (SPAN = 0.5 ± 0.15, 0.62 ± 0.35, respectively).

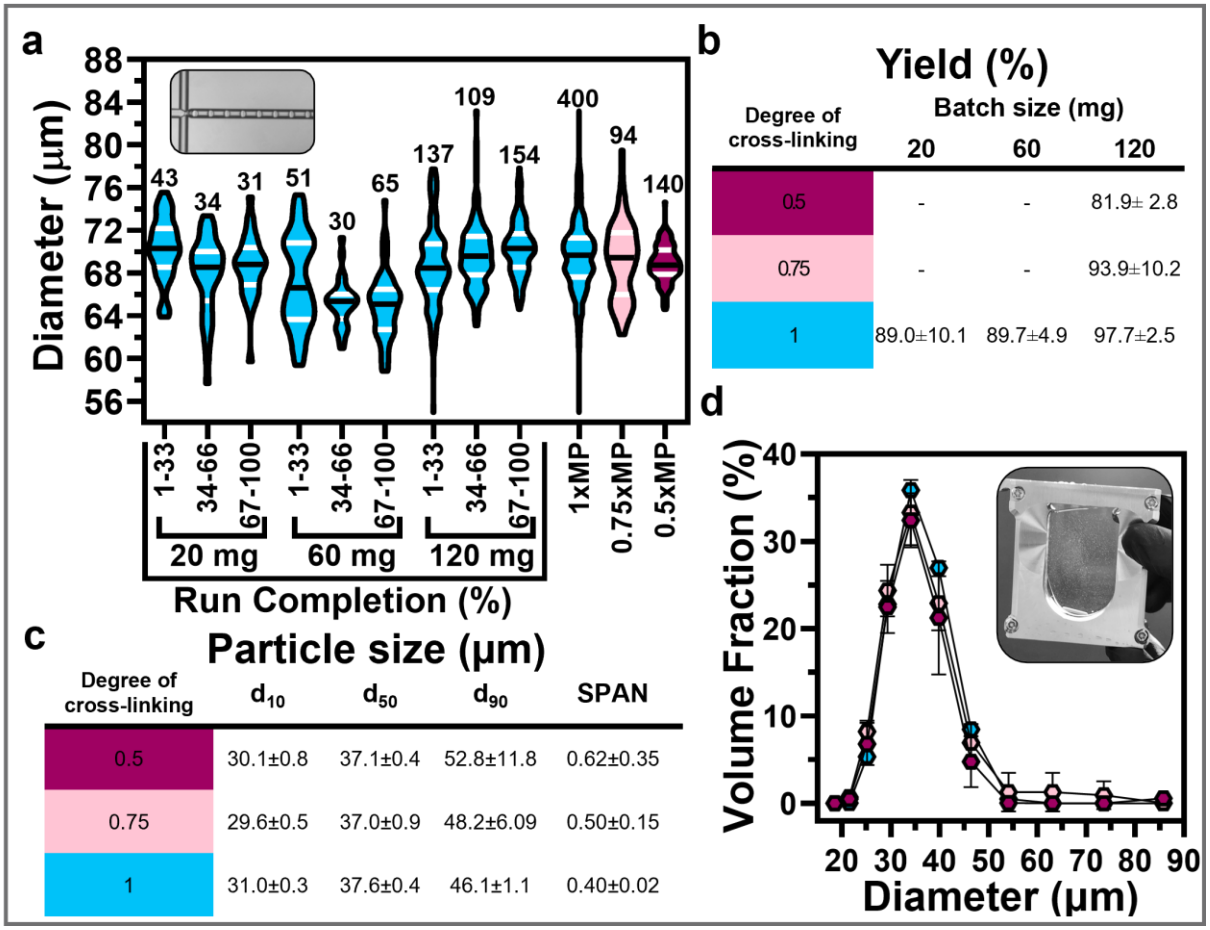

Figure 2. a Violin plots of the flow focused droplet size generated in the primary microfluidic chip at 20, 60, and 120 mg batch size for particles that had a fractional degree of cross-linking 1 and particles that had a fractional degree of cross-linking of 0.75 and 0.5, respectively (denoted 1xMP, 0.75xMP and 0.5xMP, respectively) (n = 3). The black bar denotes the median whereas the white bars show the interquartile range, the number of individual measurements is shown above. A representative image of the droplets used to generate the size measurements is also shown (top left insert). **b** The average yield for prepared xMP (n = 3 ± σ). **c** A table summarizing the distribution of xMP is where the 10th (d_{10}), 50th (d_{50}), and 90th (d_{90}) percentile diameters are shown. The SPAN is a dimensionless ratio of the difference between d_{90} and d_{10} over d_{50}. **d** Average volume weighted size distribution of xMP measured by laser light scattering (n = 3 ± σ), an image of dispersed particles is shown in the insert.

4.2 Particle Morphology

Light microscopy images (DM IL LED, Leica) confirmed the results observed by laser light scattering and showed 1xMP, 0.75xMP and 0.5xMP had a smooth morphology (**Fig. 3a**). At high magnification, scanning electron microscopy (TM4000, Hitachi) (**Fig. 3b**) showed that both 1xMP and 0.75xMP had small pores on the surface, though fewer pores were evident on the 0.75xMP surface. In contrast, 0.5xMP particles had a smoother appearance with no surface pores. Macroscopically, 1xMP was a free-flowing powder whereas 0.5xMP particles were more cohesive and adhesive. Qualitative comparison of microscopy images shows that the xMP were more monodisperse compared to similar particles prepared using bulk-emulsification [20,21].

Sectioned 1xMP showed a ~2–3 µm thick shell at the surface with voids within the intra-particle matrix (**Fig. 3c**). A shell-like layer at the particle periphery is also apparent for 0.75xMP and 0.5xMP. Consideration of cross-linking process for xMP may explain the observed morphology.

UV irradiates the droplets from the outside forming an immobilized covalent network before significant amounts of DCM have been removed. Therefore, heterogenous intra-droplet UV exposure may result in preferential cross-linking of *p*PLA chains closer to the surface forming a dense outer shell. During removal of organic solvent from PLGA droplets (i.e., hardening to form MPs), the nascent particle shrinks and transitions from a solution-, to a gel-, and then a glassy-state as the PLGA chains precipitate and anneal [67,68]. In contrast, the matrix of xMP is more restricted and cannot shrink to the same extent which is hypothesized to result in the formation of internal voids. The mass concentration of the reactive polymer solutions (i.e., *p*PLA + HDT + PT) is ~0.11 g/mL. So, the cross-linkable mass within each ~70 µm droplet (**Fig. 2a**) is approximately 19 ng (assuming incompressible fluids and isovolumetric solvation). Whilst the density of *p*PLA as received has not been characterized, the absolute density of PLGA has been reported to be 1.34 g/mL [69]. An 19 ng homogenous sphere with a density of 1.34 g/mL has a diameter of 30 µm (whereas xMP has 37–38 µm median diameter). Overall, the morphology of xMP varies with the degree of cross-linking and the intra-particle voids suggests that they may be amenable to entrap drugs for sustained release applications. To probe the internal environment of xMP, NMR analysis then compared the solid state ^{13}C NMR spectra of xMP to the solution state ^{13}C NMR spectra of PT, HDT and *p*PLA materials (**Fig. 4**).

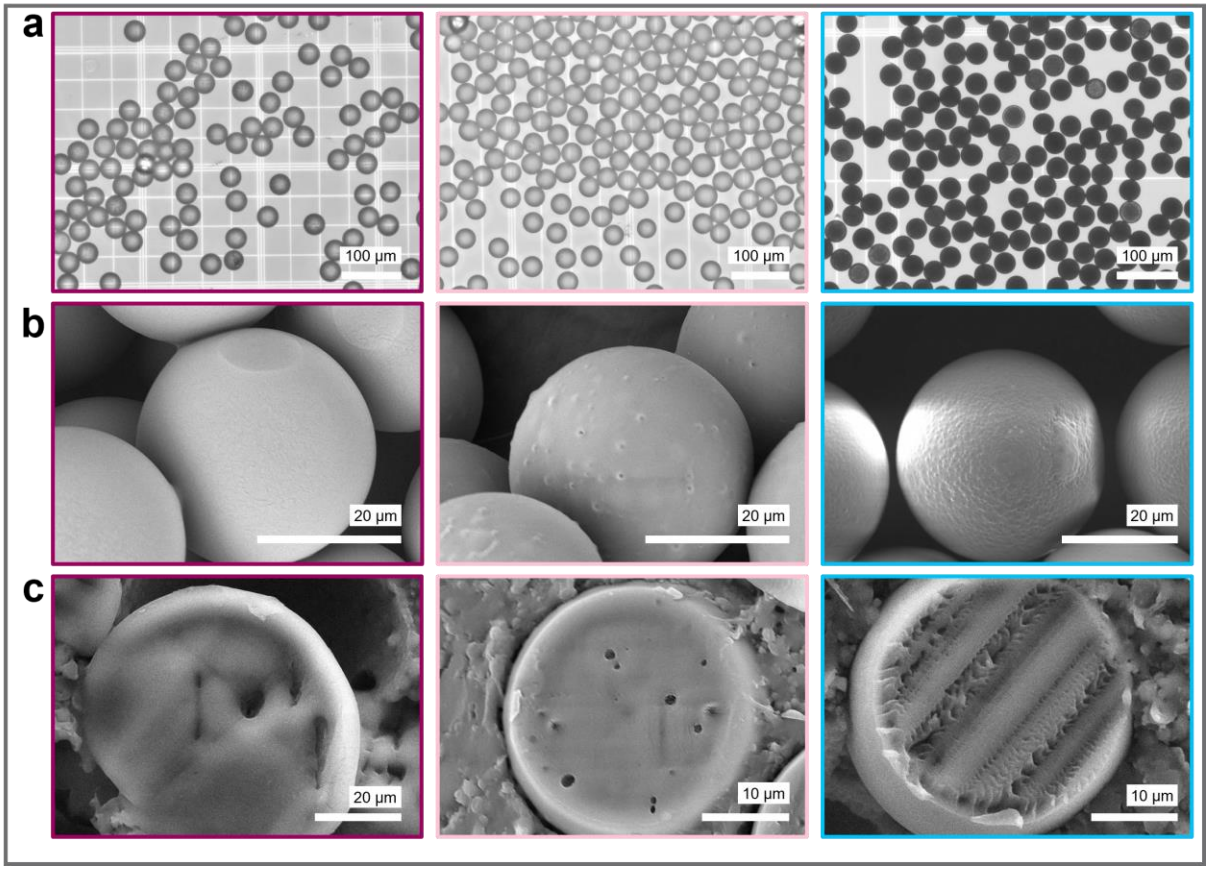

Figure 3. a Representative light microscopy images of cross-linked microparticles (xMP) suspended in water with a fractional degree of cross-linking of 0.5, 0.75 and 1 (purple, pink and blue boarders, respectively). **b** Scanning electron microscopy (SEM) images of xMP. **c** SEM images of the intra-particle morphology of sectioned xMP.

4.3 NMR Analysis

During xMP cross-linking, pendant allyl groups react with thiols (either HDT or PT) to form sulfide bonds (**Fig. 4a**). Though the stability of particles when washed with acetone (during work-up steps) qualitatively suggests that xMP were cross-linked, NMR analysis provides molecular insight into the matrix of xMP. The flow sensor accuracy results (**Fig. S1c**) imply that the exposure time was 3.1 mins rather than the targeted 3.5 mins. Nevertheless, experimental spectra agreed with the simulation of the repeating cross-linked structures suggesting inline cross-linking was complete (**Fig. 4b, c**). Characteristic olefinic ^{13}C resonances present in the *p*PLA spectrum at 119 ppm and 132 ppm were not evident in the solid state magic angle spinning (MAS) spectrum of xMP. Inline cross-linking is attractive as it ensures all particles have identical UV exposure irrespective of batch size reducing challenges when scaling manufacturing. In the current study, FEP tubing and a UV oven were used because it is easy to modify the exposure time by adjusting the tubing length. However, we recognize that dedicated serpentine microfluidic chips, which have a fixed channel length, may have advantages for inline cross-linking long-term (e.g., easier to visualize, higher UV transmission). Therefore, we have prototyped a high channel-density silica serpentine chip (i.e., 4 m long channel on 50 x 50 mm substrate) using subtractive 3D printing (LightFab) that is compatible with commercially available chip manifolds (**Fig. S3**).

The repeat structure of 0.5xMP includes sulfur-adjacent methyl and methylene groups from the inclusion of PT which are not present in 1xMP. As expected, resonances at 14.1 and 23.6 ppm corresponding to these groups increased in intensity as the degree of cross-linking reduced (i.e., for 0.75xMP and 0.5xMP). A low intensity resonance at ~123 ppm in the MAS NMR spectrum of all xMP (marked by the asterisk) is likely a spinning sideband of the carbonyl resonance at 169 ppm as samples were spun at 8 kHz, corresponding to sidebands at ~ ± 45.5 ppm in the MAS NMR spectrum. This sideband shifted by 2 kHz in the MAS spectra when 0.75xMP samples were spun at 8 kHz and 10 kHz, respectively (data not shown). The absence of olefinic peaks and varying peaks upfield (i.e., from 30–14 ppm) across the xMP NMR spectra suggested successful inline cross-linking and that 1xMP, 0.5xMP, and 0.75xMP had distinct molecular structures.

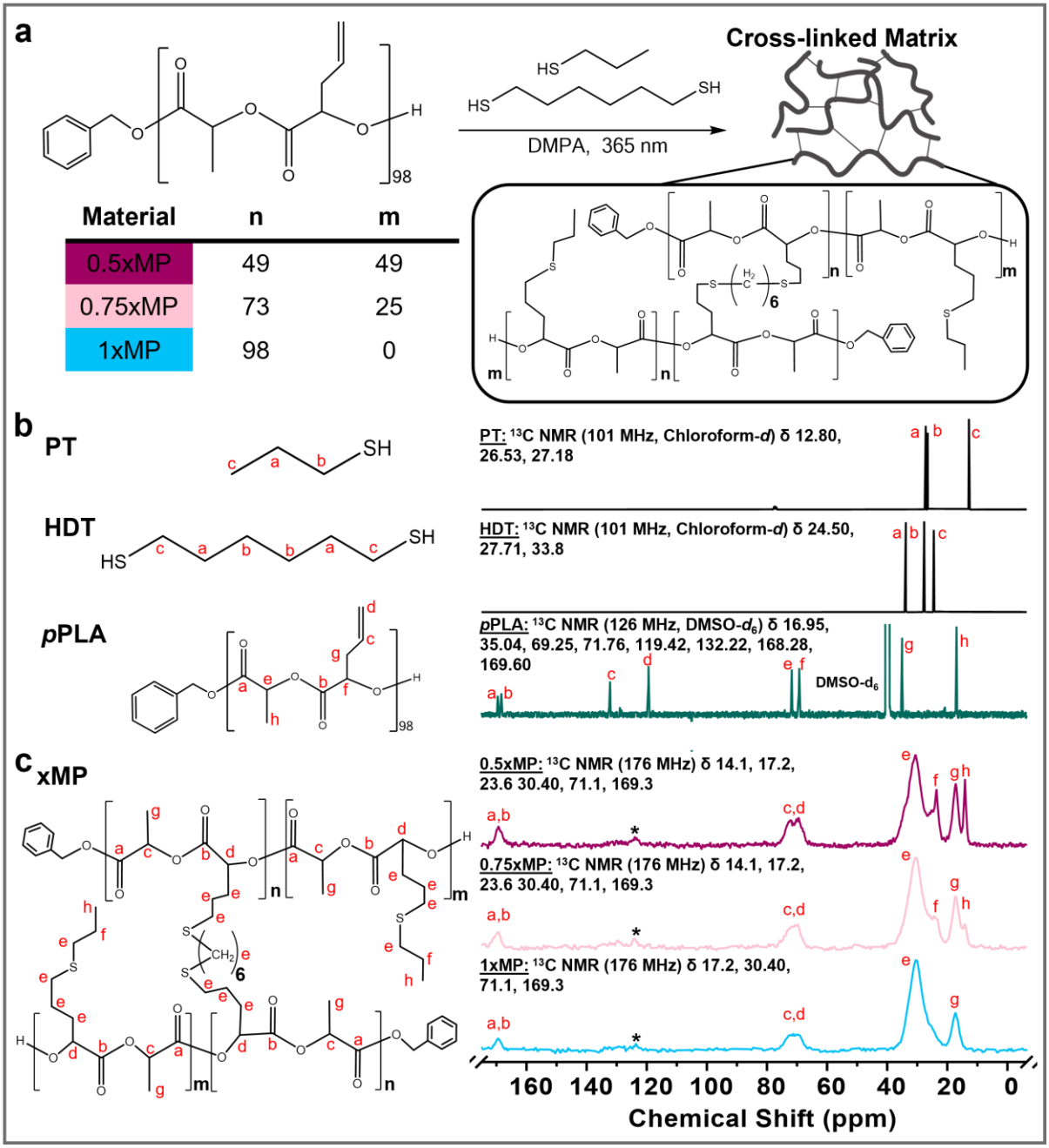

Figure 4. a Overview of the thiol-ene cross-linking reaction of poly(1-allyl-3-methyl-glycolide) (*p*PLA) with propanethiol (PT) and hexanedithiol (HDT) in the presence of 2,2-dimethoxy-2-phenylacetophenone (DMPA) under UV irradiation. The repeating structure of the cross-linked microparticles (xMP) with a fractional degree of cross-linking of 1, 0.75, and 0.5 (denoted 0.5xMP, 0.75xMP and 1xMP) is shown. **b** Solution state ^{13}C NMR spectrum of PT, HDT (dissolved in deuterated chloroform) and *p*PLA (dissolved in dimethyl sulfoxide, DMSO-d6). **c** Solid state ^{13}C NMR spectra of 0.5xMP, 0.75xMP and 1xMP. The peaks at 123 ppm marked by an asterisk are attributed as spinning sidebands.

4.4 Additional Physicochemical Properties

As expected, given the NMR analysis, infrared absorption peaks typical of olefinic groups (i.e., bending and stretching) evident in the *p*PLA material are absent in the spectra of xMP (**Fig. 5a**). The glass transition temperature (T_g) of xMP was higher than the received *p*PLA material (10.4 ±

1.0 °C). The T_g increase was proportional to the degree of cross-linking ($R^2 = 0.95$), rising by 11.3, 26.4 and 39.2 °C for 0.5xMP, 0.75xMP and 1xMP, respectively (**Fig. 5b**). This trend is consistent with other reports examining the effect of the degree of cross-linking on the T_g [70,71]. The difference in T_g between 0.5xMP and 1xMP also explains the different powder flow properties observed at room temperature.

As previously described [20,21], drug is loaded into xMP by immersion in an organic solvent which is subsequently dried. A high degree of swelling is desirable as it will increase the amount of drug that penetrates the xMP. Therefore, the swelling of xMP was characterized in three solvents: EA, THF and DCM. The swelling of the xMP was inversely proportional to the squared difference in Hildebrand solubility parameters (**Fig. 5c**) which is consistent with previous literature [72]. Representative microscopy images of 1xMP in various solvents illustrate this trend (**Fig 5c**). When dispersed in DCM the diameter of 1xMP was 70 ± 1 µm, similar compared to the initial droplet diameter (**Fig. 2a**). The particles are amenable to drug loading via swelling as it is reversible (i.e., xMP shrinks as the solvent evaporates). As the degree of cross-linking reduced, the swelling of xMP in organic solvent increased, consistent with previous studies [73]. To ensure xMP integrity in organic solvent, a minimum degree of cross-linking >0.2 is required. During preliminary studies, 0.2xMP ruptured due to excess swelling when immersed in DCM (**Fig. S4**). Taken together, the spectral, thermal, and swelling characterization of xMP indicate it is a platform with which the physicochemical properties can be easily tuned to load a range of drugs as required.

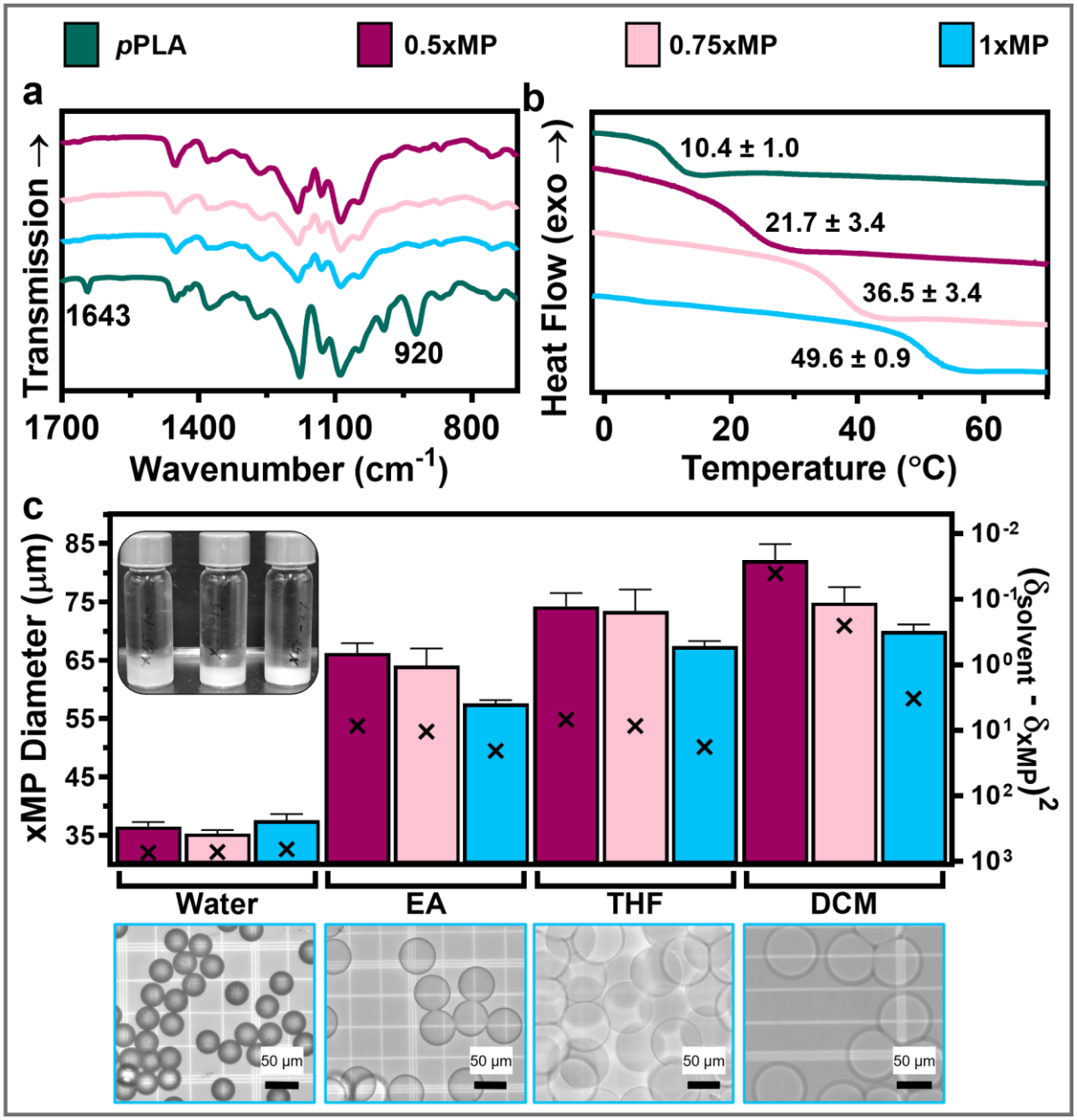

Figure 5. a Infrared spectra of poly(1-allyl-3-methyl-glycolide) (*p*PLA) material as received and of cross-linked microparticles (xMP) with a fractional degree of cross-linking of 0.5, 0.75 and 1 (0.5xMP, 0.75xMP, 1xMP, respectively). Absorptions at 1643 and 920 cm^{-1} are attributed to vinyl stretching and bending, respectively. **b** Thermograms of *p*PLA and xMP with glass transition temperatures (T_g) shown indicated (n = 3 ± σ). **c** Bar chart showing the average diameter of xMP, when immersed in water, tetrahydrofuran (THF), and dichloromethane (DCM) plotted on the left axis (n = 3 ± σ). The squared difference between the Hildebrand solubility parameter of the solvent ($\delta_{solvent}$) and xMP (δ_{xMP}) is shown by the crosses (right axis). The insert shows 0.5xMP. 0.75xMP and 1xMP batches (left to right) in acetone during particle workup, illustrating the effect of the degree of cross-linking while representative light microscopy images of 1xMP below show the effect of different solvents.

4.5 Drug loading

The swelling properties of xMP suggested that they were amenable to load celecoxib (CXB). The poor water solubility as well as dose-limiting gastro and cardio-vascular toxicity (when

administered orally) make CXB attractive to formulate as an LAI [74]. Though xMP showed the greatest degree of swelling in DCM, THF was selected as the loading solvent as xMP floated in DCM (**Fig. 6a**). Both 5 and 40wt% initial CXB was added to the xMP (denoted xMP5 and xMP40, respectively). For xMP5, drug loading efficiency decreased with increasing cross-linking, ranging from 89 ± 10 to 79 ± 8 % for 0.5xMP and 1xMP, respectively (**Fig. 6b**). xMP40 particles showed a similar trend (with loading efficiencies ranging from 88 ± 10 to 75 ± 5 %). The decrease in CXB loading with increased cross-linking is likely due to reduced swelling in THF (**Fig. 5c**). Thermal analysis showed T_g increased for 0.5xMP5 but decreased for 1xMP5 compared to the corresponding non-loaded xMP, whereas all xMP40 showed an increase in the T_g (**Fig. 6c**). Weak melting peaks at 142.1, 144.5 and 149.5 °C for 0.5xMP40, 0.75xMP40 and 1xMP40, respectively, increased with the degree of cross-linking but were lower than the melting point of pure CXB (163.1 ± 0.1 °C, **Fig. S5g**).

Electron microscopy revealed that higher CXB loading in 0.5xMP resulted in less spherical particles and increased surface pores (**Fig 6d**). In contrast, 1xMP remained spherical but exhibited needle-like structures on the surface at higher CXB content (i.e., 1xMP40). The internal morphology was more heterogenous across individual CXB-loaded particles than non-loaded xMP. Generally, higher CXB content increased the number of internal voids within the particles (**Fig. 6e**). Both the degree of cross-linking and the initial CXB added modulated loading efficiency, thermal properties and particle morphology. Beyond the cross-linking and drug loading design spaces, many process parameters described in the literature (e.g., chip junction geometry, flow rate ratio, sample fluid composition, surfactant composition) can also be varied as a means to tailor xMP properties. For instance, cross-linked particles manufactured using a preliminary microfluidic system with a 15% (w/v) *p*PLA solution showed reduced swelling and drug loading efficiency (**Fig. S5**) compared to 1xMP manufactured with a 7.5% (w/v) *p*PLA solution.

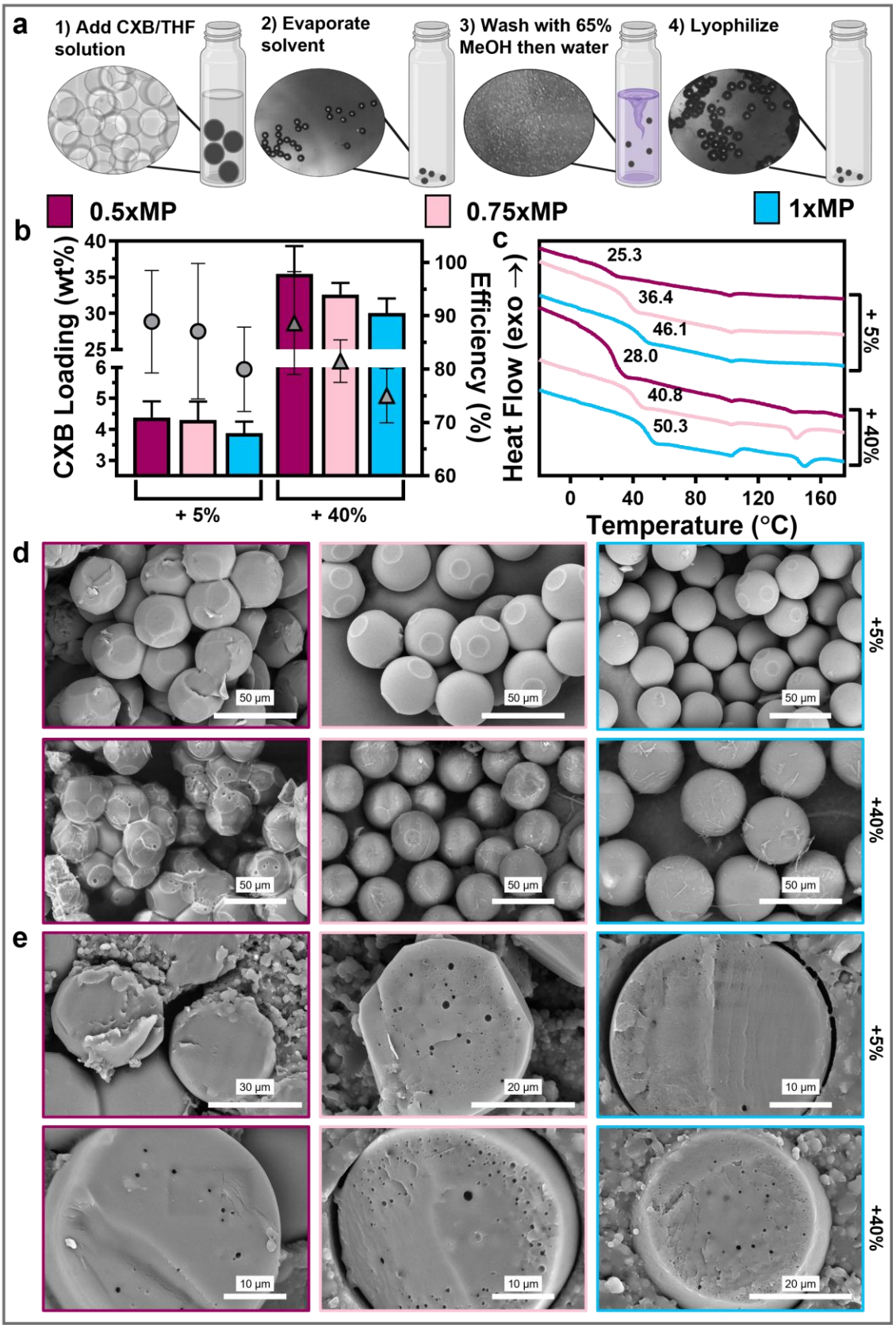

Figure 6. a Cartoon overview of the main process steps to post-load cross-linked microparticles (xMP) with the drug celecoxib (CXB). **b** Bar chart showing the CXB content of xMP with 0.5, 0.75, and 1 fractional degree of cross-linking (0.5xMP, 0.75xMP, and 1xMP, respectively) when 5 and 40wt% CXB is added (bars, left axis) and loading efficiency (symbols, right axis) ($n = 3 \pm \sigma$). **c** Thermograms of the CXB-loaded xMPs with the glass transition temperature indicated. **d** Scanning electron microscopy (SEM) images of xMPs loaded with 5wt% (upper) and 40wt% (lower) CXB. **e** Corresponding SEM images of sectioned particles.

4.6 In Vitro Release

The *in vitro* release of xMP5 and xMP40 was characterized using a sample-and-separate method for up to 72 days (**Fig. 7**). For xMP5 formulations, the release rate was inversely proportional to the degree of cross-linking, ranging from 93 ± 11 to 27 ± 3 % release at 24 days for 0.5xMP5 and 1xMP5, respectively (**Fig. 7a**). A similar trend was observed for xMP40 with 82 ± 5 and 14.3 ± 5 % released at 24 days for 0.5xMP and 1xMP, respectively (**Fig. 7b**). Over 72 days, 1xMP5 and 1xMP40 showed 82 ± 19 and 26 ± 4 % total release, respectively. CXB was stable in the release media (**Fig. S6b**) and the remaining CXB was extracted from xMP post-study (**Table S1**). The degradation of the particles was not examined for CXB-loaded xMP. However, the degradation of poly(lactide) has been well-explored [75] and cross-linked poly(lactide-*b*-ethylene glycol-*b*-lactide) based hydrogels have shown degradation rates inversely proportional to the degree of cross-linking [76–78]. Therefore, we expect a similar trend in terms of relative degradation rate for xMP described in the current study; quantification of xMP degradation kinetics will be carried out in future work.

The loading and *in vitro* release of CXB from xMP is comparable to CXB-loaded MPs which have shown efficacy treating osteoarthritis in rats [79] and dogs [74]. There have been a number of studies preparing CXB-loaded PLGA MPs using emulsion-based [80–84] and spray-based [85–88] methods. While it is difficult to make direct comparisons due to multiple differences across formulations (e.g., polymer Mw, particle size, etc.), in general, they report lower loading and more rapid *in vitro* release compared to 1xMP40. Since the degree of cross-linking is a continuous design parameter, it is feasible to achieve any release profile between 0.5xMP and 1xMP by adjusting the stoichiometry of HDT and PT.

The value proposition for using microfluidic manufactured xMP in LAI applications is two-fold. As proof of concept, we have shown that the degree of cross-linking can tailor xMP properties. Additionally, the structure of the cross-linker can be modulated. For example, preliminary data characterizing particles cross-linked with pentaerythritol tetrakis(3-mercaptopropionate) (denoted $0.75x^2$MP, **Fig. S7**) show that inclusion of a tetra-functional, hydrolysable cross-linker increased T_g and lowered the *in vitro* release rate compared to 0.75xMP. Since thiol-ene click chemistry is highly established, many diverse thiols are readily available. Second, xMP stability in organic solvent facilitates drug loading post-matrix production in two independent steps. While this does increase the complexity of the process overall, decoupling the xMP production from drug loading affords flexibility in the design space which can be optimized independently of xMP production.

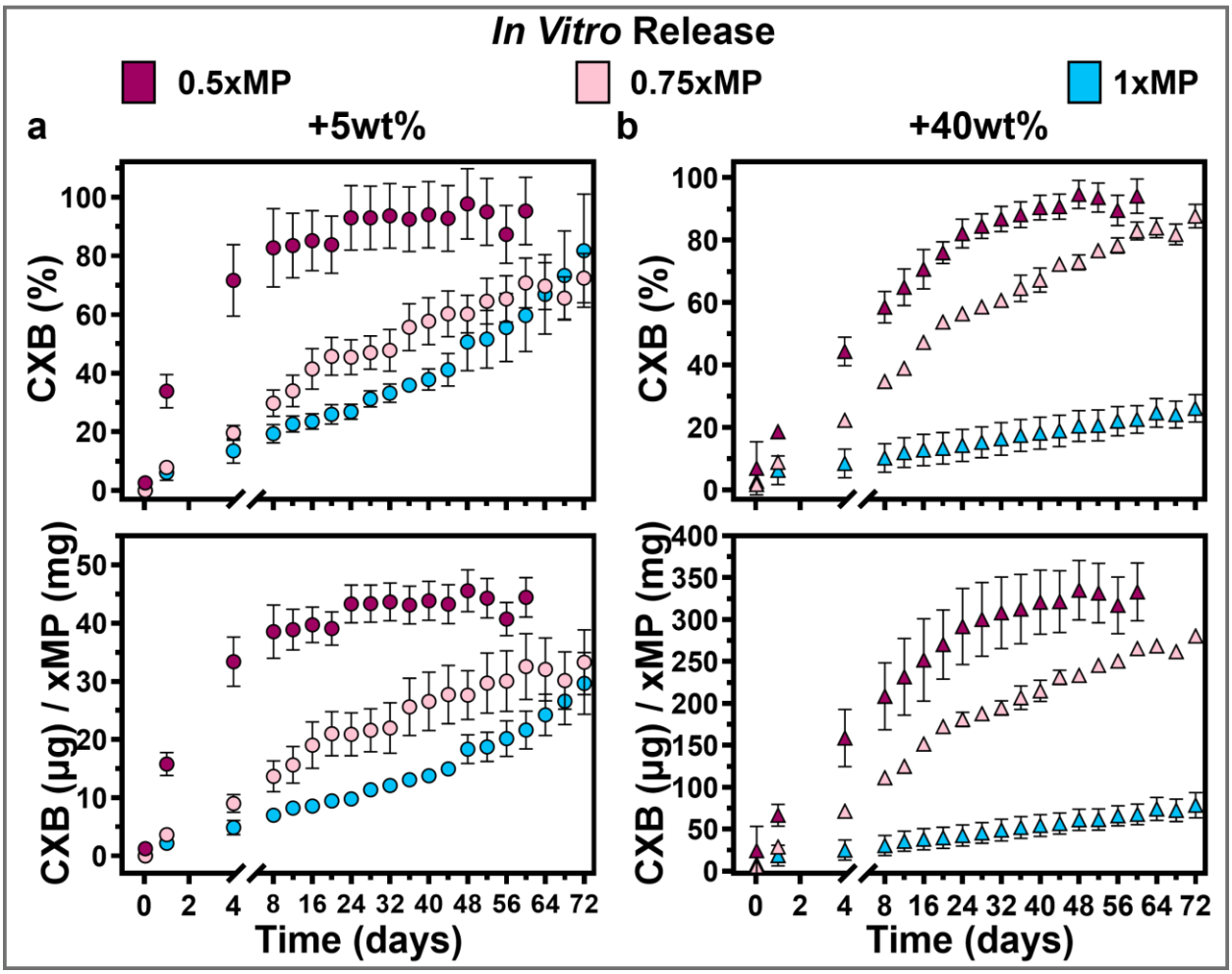

Figure 7. Average fractional and absolute *in vitro* release of cross-linked microparticles with a fractional degree of cross-linking of 0.5, 0.75, 1 (0.5xMP, 0.75xMP and 1xMP, respectively) when 5wt% (**a**) and 40wt% (**b**) celecoxib (CXB) was added during loading (n = 3 ± σ, 0.5xMP and 1xMP formulations loaded with 5wt% CXB are n = 2 ± σ).

5. CONCLUSIONS

The microfluidic technique detailed herein has demonstrated capabilities to manufacture xMP by generating monodisperse reactive droplets and cross-linking them via inline UV exposure. Overall, production rates for xMP of 60 mg/hr, at batch sizes from 20–120 mg with 89–98% yields were achieved. Robust deployment of microfluidic techniques for xMP manufacturing requires both chemical and mechanical considerations of the whole system as well as methodological considerations beyond droplet generation. Physicochemical characterization of xMP indicated that the cross-linking reaction was both achievable and that the degree of cross-linking was easily tunable. This tunable cross-linking enabled precise modulation of key material properties such as *in vitro* release rate. The three distinct design spaces (microfluidic process, cross-linking chemistry, and drug loading) provide xMP with a wide range of tunable properties. Therefore, microfluidic-manufactured xMP has the potential to be a platform LAI technology for sustained release of many drugs across various indications.

AUTHOR INFORMATION

Corresponding Authors

Christine Allen - Leslie Dan Faculty of Pharmacy, University of Toronto, Toronto, M5S 3M2. Email: cj.allen@utoronto.ca
Jack R. Bufton - Leslie Dan Faculty of Pharmacy, University of Toronto, Toronto, M5S 3M2. Email: jack.bufton@mail.utoronto.ca
Authors
Darcy C. Burns - CSICOMP NMR Facility, Department of Chemistry, University of Toronto, Toronto, ON, M5S 3H6, Canada
Jeffery Watchorn - Acceleration Consortium, Toronto, ON, M5S 3H6, Canada
Seoyeon Lee - Leslie Dan Faculty of Pharmacy, University of Toronto, Toronto, M5S 3M2.

AUTHOR CONTRIBUTIONS

Jack R. Bufton: Conceptualization, Investigation, Visualization, Writing – original draft, Writing – review & editing. **Darcy C. Burns:** Investigation, Writing – review & editing. **Jeffrey Watchorn:** Writing – review & editing **Seoyeon Lee** – Investigation, Writing – review & editing. **Christine Allen:** Project administration, Supervision, Writing – review & editing, Funding acquisition.

ACKNOWLEDGMENTS

Figures were created with Biorender.com and Prism v10. J.B. acknowledges a Dean's scholarship from the Leslie Dan Faculty of Pharmacy. This work was funded by an NSERC discovery grant awarded to C.A. (RGPIN-2022-04910). The authors acknowledge the Centre for Research in Applied Fluidic Technologies (CRAFT) device foundry facility for assistance with the electron microscopy imaging studies and silica 3D printing. J.B. would like to thank Angela Niu for her assistance with the CAD of the serpentine chip. The authors also acknowledge the Centre for Spectroscopic Investigation of Complex Organic Molecules and Polymers (CSICOMP) for NMR studies. This research was undertaken thanks in part to funding provided to the University of Toronto's Acceleration Consortium from the Canada First Research Excellence Fund (CFREF).

ABBREVIATIONS

Microparticles (MPs), long-acting injectables (LAIs), United States Food and Drug Administration (FDA), poly(lactide-*co*-glycolide) (PLGA), cross-linked microparticle (xMP), poly(1-allyl-3-methyl-glycolide) (*p*PLA), hexanedithiol (HDT), pronpanethiol (PT), celecoxib (CXB), methanol (MeOH), dichloromethane (DCM), poly(vinyl alcohol) (PVA), deuterated dimethyl sulfoxide (DMSO-d6), tetrahydrofuran (THF), ethyl acetate (EA), 2,2-dimethoxy-2-phenylacetophenone (DMPA), trifluoroacetic acid (TFA), phosphate buffered saline (PBS), sodium dodecyl sulfate (SDS), ethylene tetrafluoroethylene (ETFE), fluorinated ethylene propylene (FEP), poly(tetrafluoroethylene) (PTFE), poly(ether-ether ketone) (PEEK), high pressure liquid chromotography (HPLC), deionized water (DI), nuclear magnetic resnoance (MNR), ultraviolet light (UV), magic angle spinning (MAS).

6. REFERENCES

[1] M.H. Rafiee, B.K. Abdul Rasool, An Overview of Microparticulate Drug Delivery System and its Extensive Therapeutic Applications in Diabetes, Adv Pharm Bull 12 (2022) 730–746. https://doi.org/10.34172/apb.2022.075.
[2] K. Park, S. Skidmore, J. Hadar, J. Garner, H. Park, A. Otte, B.K. Soh, G. Yoon, D. Yu, Y. Yun, B.K. Lee, X. Jiang, Y. Wang, Injectable, long-acting PLGA formulations: Analyzing PLGA and understanding microparticle formation, Journal of Controlled Release 304 (2019) 125–134. https://doi.org/10.1016/j.jconrel.2019.05.003.

[3] C.I. Nkanga, A. Fisch, M. Rad-Malekshahi, M.D. Romic, B. Kittel, T. Ullrich, J. Wang, R.W.M. Krause, S. Adler, T. Lammers, W.E. Hennink, F. Ramazani, Clinically established biodegradable long acting injectables: An industry perspective, Adv Drug Deliv Rev 167 (2020) 19–46. https://doi.org/10.1016/j.addr.2020.11.008.
[4] A. Butreddy, R.P. Gaddam, N. Kommineni, N. Dudhipala, C. Voshavar, PLGA/PLA-Based Long-Acting Injectable Depot Microspheres in Clinical Use: Production and Characterization Overview for Protein/Peptide Delivery, Int J Mol Sci 22 (2021) 8884. https://doi.org/10.3390/ijms22168884.
[5] C.Y. Wong, H. Al-Salami, C.R. Dass, Microparticles, microcapsules and microspheres: A review of recent developments and prospects for oral delivery of insulin, Int J Pharm 537 (2018) 223–244. https://doi.org/10.1016/j.ijpharm.2017.12.036.
[6] Mathematical models of drug release, in: Strategies to Modify the Drug Release from Pharmaceutical Systems, Elsevier, 2015: pp. 63–86. https://doi.org/10.1016/B978-0-08-100092-2.00005-9.
[7] D. Lin, P. Thompson-Leduc, I. Ghelerter, H. Nguyen, M.-H. Lafeuille, C. Benson, P. Mavros, P. Lefebvre, Real-World Evidence of the Clinical and Economic Impact of Long-Acting Injectable Versus Oral Antipsychotics Among Patients with Schizophrenia in the United States: A Systematic Review and Meta-Analysis, CNS Drugs 35 (2021) 469–481. https://doi.org/10.1007/s40263-021-00815-y.
[8] S. Kheloussi, J. Oberlin, M. Trauger, N.D. Testa, Clinical and economic impact of long-acting injectable antipsychotics in patients previously treated with short-acting oral antipsychotics, J Manag Care Spec Pharm 28 (2022) 1130–1137. https://doi.org/10.18553/jmcp.2022.28.10.1130.
[9] T.R. Einarson, S. Maia-Lopes, P. Goswami, B.G. Bereza, K. Van Impe, Economic analysis of paliperidone long-acting injectable for chronic schizophrenia in Portugal, J Med Econ 19 (2016) 913–921. https://doi.org/10.1080/13696998.2016.1184156.
[10] K. Chwalisz, Clinical development of the GnRH agonist leuprolide acetate depot, F&S Reports 4 (2023) 33. https://doi.org/10.1016/j.xfre.2022.11.011.
[11] R. Bhujel, R. Maharjan, N.A. Kim, S.H. Jeong, Practical quality attributes of polymeric microparticles with current understanding and future perspectives, Journal of Drug Delivery Science and Technology 64 (2021) 102608. https://doi.org/10.1016/j.jddst.2021.102608.
[12] B. Wan, Q. Bao, D. Burgess, Long-acting PLGA microspheres: advances in excipient and product analysis toward improved product understanding, Advanced Drug Delivery Reviews (2023) 114857. https://doi.org/10.1016/j.addr.2023.114857.
[13] A. Schoubben, M. Ricci, S. Giovagnoli, Meeting the unmet: from traditional to cutting-edge techniques for poly lactide and poly lactide-co-glycolide microparticle manufacturing, J. Pharm. Investig. 49 (2019) 381–404. https://doi.org/10.1007/s40005-019-00446-y.
[14] M.N. O'Brien, W. Jiang, Y. Wang, D.M. Loffredo, Challenges and opportunities in the development of complex generic long-acting injectable drug products, Journal of Controlled Release 336 (2021) 144–158. https://doi.org/10.1016/j.jconrel.2021.06.017.
[15] T.K. Dash, V.B. Konkimalla, Poly-ϵ-caprolactone based formulations for drug delivery and tissue engineering: A review, Journal of Controlled Release 158 (2012) 15–33. https://doi.org/10.1016/j.jconrel.2011.09.064.
[16] A. Bettencourt, A.J. Almeida, Poly(methyl methacrylate) particulate carriers in drug delivery, Journal of Microencapsulation 29 (2012) 353–367. https://doi.org/10.3109/02652048.2011.651500.
[17] J. Li, D.J. Mooney, Designing hydrogels for controlled drug delivery, Nat Rev Mater 1 (2016) 1–17. https://doi.org/10.1038/natrevmats.2016.71.
[18] X. Tong, W. Pan, T. Su, M. Zhang, W. Dong, X. Qi, Recent advances in natural polymer-based drug delivery systems, Reactive and Functional Polymers 148 (2020) 104501. https://doi.org/10.1016/j.reactfunctpolym.2020.104501.
[19] T. Andreani, A.M. Silva, E.B. Souto, Silica-based matrices: State of the art and new perspectives for therapeutic drug delivery, Biotechnology and Applied Biochemistry 62 (2015) 754–764. https://doi.org/10.1002/bab.1322.
[20] Z. Bao, S. Jung, J. Bufton, J.C. Evans, D.J. Aguiar, C. Allen, Poly(δ-valerolactone-co-allyl-δ-valerolactone) cross-linked microparticles: Formulation, characterization and biocompatibility, Journal of Pharmaceutical Sciences (2021). https://doi.org/10.1016/j.xphs.2021.03.009.
[21] Z. Bao, S. Jung, J. Bufton, P. Bannigan, D.J. Aguiar, C. Allen, Data evaluating triamcinolone acetonide and triamcinolone hexacetonide loaded poly(δ-valerolactone-co-allyl-δ-valerolactone) microparticles, Data in Brief 48 (2023) 109032. https://doi.org/10.1016/j.dib.2023.109032.
[22] K. Park, A. Otte, F. Sharifi, J. Garner, S. Skidmore, H. Park, Y.K. Jhon, B. Qin, Y. Wang, Formulation composition, manufacturing process, and characterization of poly(lactide-co-glycolide) microparticles, Journal of Controlled Release 329 (2021) 1150–1161. https://doi.org/10.1016/j.jconrel.2020.10.044.

[23] M. Chen, G. Bolognesi, G.T. Vladisavljević, Crosslinking Strategies for the Microfluidic Production of Microgels, Molecules 26 (2021) 3752. https://doi.org/10.3390/molecules26123752.
[24] P. Cawley, I. Wilkinson, R.J. Ross, Developing long-acting growth hormone formulations, Clin Endocrinol (Oxf) 79 (2013) 305–309. https://doi.org/10.1111/cen.12240.
[25] Y. Cai, M. Xu, M. Yuan, Z. Liu, W. Yuan, Developments in human growth hormone preparations: sustained-release, prolonged half-life, novel injection devices, and alternative delivery routes, International Journal of Nanomedicine 9 (2014) 3527–3538. https://doi.org/10.2147/IJN.S63507.
[26] F. Molavi, M. Barzegar-Jalali, H. Hamishehkar, Polyester based polymeric nano and microparticles for pharmaceutical purposes: A review on formulation approaches, Journal of Controlled Release 320 (2020) 265–282. https://doi.org/10.1016/j.jconrel.2020.01.028.
[27] W.J. Duncanson, M. Zieringer, O. Wagner, J.N. Wilking, A. Abbaspourrad, R. Haag, D.A. Weitz, Microfluidic synthesis of monodisperse porous microspheres with size-tunable pores, Soft Matter 8 (2012) 10636–10640.
[28] C. Zhu, H. Yang, L. Shen, Z. Zheng, S. Zhao, Q. Li, F. Yu, L. Cen, Microfluidic preparation of PLGA microspheres as cell carriers with sustainable Rapa release, Journal of Biomaterials Science, Polymer Edition 30 (2019) 737–755. https://doi.org/10.1080/09205063.2019.1602930.
[29] E. Jafarifar, M. Hajialyani, M. Akbari, M. Rahimi, Y. Shokoohinia, A. Fattahi, Preparation of a reproducible long-acting formulation of risperidone-loaded PLGA microspheres using microfluidic method, Pharmaceutical Development and Technology 22 (2017) 836–843. https://doi.org/10.1080/10837450.2016.1221426.
[30] Y. Su, J. Liu, S. Tan, W. Liu, R. Wang, C. Chen, PLGA sustained-release microspheres loaded with an insoluble small-molecule drug: microfluidic-based preparation, optimization, characterization, and evaluation in vitro and in vivo, Drug Delivery 29 (2022) 1437–1446. https://doi.org/10.1080/10717544.2022.2072413.
[31] H.-G. Kim, K.-M. Kim, Y.H. Kim, S.H. Lee, G.M. Kim, Preparation of Monodisperse ENX-Loaded PLGA Microspheres Using a Microfluidic Flow-Focusing Device, Journal of Biobased Materials and Bioenergy 7 (2013) 108–114. https://doi.org/10.1166/jbmb.2013.1263.
[32] Q. Xu, M. Hashimoto, T.T. Dang, T. Hoare, D.S. Kohane, G.M. Whitesides, R. Langer, D.G. Anderson, Preparation of Monodisperse Biodegradable Polymer Microparticles Using a Microfluidic Flow-Focusing Device for Controlled Drug Delivery, Small 5 (2009) 1575–1581. https://doi.org/10.1002/smll.200801855.
[33] K. Keohane, D. Brennan, P. Galvin, B.T. Griffin, Silicon microfluidic flow focusing devices for the production of size-controlled PLGA based drug loaded microparticles, International Journal of Pharmaceutics 467 (2014) 60–69. https://doi.org/10.1016/j.ijpharm.2014.03.051.
[34] S.A. Damiati, S. Damiati, Microfluidic Synthesis of Indomethacin-Loaded PLGA Microparticles Optimized by Machine Learning, Frontiers in Molecular Biosciences 8 (2021). https://www.frontiersin.org/articles/10.3389/fmolb.2021.677547 (accessed July 21, 2022).
[35] N. Yonet-Tanyeri, M. Amer, S.C. Balmert, E. Korkmaz, L.D.Jr. Falo, S.R. Little, Microfluidic Systems For Manufacturing of Microparticle-Based Drug-Delivery Systems: Design, Construction, and Operation, ACS Biomater. Sci. Eng. 8 (2022) 2864–2877. https://doi.org/10.1021/acsbiomaterials.2c00066.
[36] J.H. Kim, C.H. Ryu, C.H. Chon, S. Kim, S. Lee, R. Maharjan, N.A. Kim, S.H. Jeong, Three months extended-release microspheres prepared by multi-microchannel microfluidics in beagle dog models, International Journal of Pharmaceutics 608 (2021) 121039. https://doi.org/10.1016/j.ijpharm.2021.121039.
[37] T. He, Q. Liang, K. Zhang, X. Mu, T. Luo, Y. Wang, G. Luo, A modified microfluidic chip for fabrication of paclitaxel-loaded poly(l-lactic acid) microspheres, Microfluid Nanofluid 10 (2011) 1289–1298. https://doi.org/10.1007/s10404-010-0760-7.
[38] H. Dong, G. Tang, T. Ma, X. Cao, One-step fabrication of inorganic/organic hybrid microspheres with tunable surface texture for controlled drug release application, Journal of Materials Science: Materials in Medicine 27 (2016) 1–8.
[39] A. Perez, R. Hernandez, D. Velasco, D. Voicu, C. Mijangos, Poly (lactic-co-glycolic acid) particles prepared by microfluidics and conventional methods. Modulated particle size and rheology, Journal of Colloid and Interface Science 441 (2015) 90–97.
[40] R. Samimi, M. Salarian, W.Z. Xu, E.M. Lui, P.A. Charpentier, Encapsulation of acetyl ginsenoside Rb1 within monodisperse poly (dl-lactide-co-glycolide) microspheres using a microfluidic device, Industrial & Engineering Chemistry Research 53 (2014) 11333–11344.
[41] L. Montazeri, S. Bonakdar, M. Taghipour, P. Renaud, H. Baharvand, Modification of PDMS to fabricate PLGA microparticles by a double emulsion method in a single microfluidic device, Lab on a Chip 16 (2016) 2596–2600.

[42] Y.-S. Lin, C.-H. Yang, C.-Y. Wang, F.-R. Chang, K.-S. Huang, W.-C. Hsieh, An aluminum microfluidic chip fabrication using a convenient micromilling process for fluorescent poly (DL-lactide-co-glycolide) microparticle generation, Sensors 12 (2012) 1455–1467.
[43] M.A. Holgado, M.J. Cózar-Bernal, S. Salas, J.L. Arias, J. Alvarez-Fuentes, M. Fernández-Arévalo, Protein-loaded PLGA microparticles engineered by flow focusing: physicochemical characterization and protein detection by reversed-phase HPLC, International Journal of Pharmaceutics 380 (2009) 147–154.
[44] R. Vasiliauskas, D. Liu, S. Cito, H. Zhang, M.-A. Shahbazi, T. Sikanen, L. Mazutis, H.A. Santos, Simple Microfluidic Approach to Fabricate Monodisperse Hollow Microparticles for Multidrug Delivery, ACS Appl. Mater. Interfaces 7 (2015) 14822–14832. https://doi.org/10.1021/acsami.5b04824.
[45] M.J. Cózar-Bernal, M.A. Holgado, J.L. Arias, I. Muñoz-Rubio, L. Martín-Banderas, J. Alvarez-Fuentes, M. Fernández-Arévalo, Insulin-loaded PLGA microparticles: flow focusing versus double emulsion/solvent evaporation, Journal of Microencapsulation 28 (2011) 430–441.
[46] I. Morita, Y. Ando, Y.J. Heo, Microsphere formation using SIFEL microfluidic devices with organic-solvent resistance, Journal of Advanced Mechanical Design, Systems, and Manufacturing 11 (2017) JAMDSM0031–JAMDSM0031.
[47] T. Schneider, G.H. Chapman, U.O. Häfeli, Effects of chemical and physical parameters in the generation of microspheres by hydrodynamic flow focusing, Colloids and Surfaces B: Biointerfaces 87 (2011) 361–368.
[48] M.A. Holgado, J.L. Arias, M.J. Cózar, J. Alvarez-Fuentes, A.M. Gañán-Calvo, M. Fernández-Arévalo, Synthesis of lidocaine-loaded PLGA microparticles by flow focusing: effects on drug loading and release properties, International Journal of Pharmaceutics 358 (2008) 27–35.
[49] A. Forigua, A. Dalili, R. Kirsch, S.M. Willerth, K.S. Elvira, Microfluidic Generation of Therapeutically Relevant Polycaprolactone (PCL) Microparticles: Computational and Experimental Approaches, ACS Appl. Polym. Mater. 4 (2022) 7004–7013. https://doi.org/10.1021/acsapm.2c00943.
[50] M. Hussain, J. Xie, Z. Hou, K. Shezad, J. Xu, K. Wang, Y. Gao, L. Shen, J. Zhu, Regulation of Drug Release by Tuning Surface Textures of Biodegradable Polymer Microparticles, ACS Appl. Mater. Interfaces 9 (2017) 14391–14400. https://doi.org/10.1021/acsami.7b02002.
[51] D. Baah, T. Floyd-Smith, Microfluidics for particle synthesis from photocrosslinkable materials, Microfluid Nanofluid 17 (2014) 431–455. https://doi.org/10.1007/s10404-014-1333-y.
[52] C. Zhang, L. Yang, F. Wan, H. Bera, D. Cun, J. Rantanen, M. Yang, Quality by design thinking in the development of long-acting injectable PLGA/PLA-based microspheres for peptide and protein drug delivery, Int J Pharm 585 (2020) 119441. https://doi.org/10.1016/j.ijpharm.2020.119441.
[53] E.W.Q. Yeap, D.Z.L. Ng, D. Lai, D.J. Ertl, S. Sharpe, S.A. Khan, Continuous Flow Droplet-Based Crystallization Platform for Producing Spherical Drug Microparticles, Org. Process Res. Dev. 23 (2019) 93–101. https://doi.org/10.1021/acs.oprd.8b00314.
[54] C. Hu, Reactor design and selection for effective continuous manufacturing of pharmaceuticals, J Flow Chem 11 (2021) 243–263. https://doi.org/10.1007/s41981-021-00164-3.
[55] W. Li, L. Zhang, X. Ge, B. Xu, W. Zhang, L. Qu, C.-H. Choi, J. Xu, A. Zhang, H. Lee, D. A. Weitz, Microfluidic fabrication of microparticles for biomedical applications, Chemical Society Reviews 47 (2018) 5646–5683. https://doi.org/10.1039/C7CS00263G.
[56] P. Zhu, L. Wang, Passive and active droplet generation with microfluidics: a review, Lab Chip 17 (2016) 34–75. https://doi.org/10.1039/c6lc01018k.
[57] A.S. Utada, A. Fernandez-Nieves, H.A. Stone, D.A. Weitz, Dripping to jetting transitions in coflowing liquid streams, Phys Rev Lett 99 (2007) 094502. https://doi.org/10.1103/PhysRevLett.99.094502.
[58] A. Kalantarifard, E. Alizadeh-Haghighi, A. Saateh, C. Elbuken, Theoretical and experimental limits of monodisperse droplet generation, Chemical Engineering Science 229 (2021) 116093. https://doi.org/10.1016/j.ces.2020.116093.
[59] K.W. Oh, K. Lee, B. Ahn, E.P. Furlani, Design of pressure-driven microfluidic networks using electric circuit analogy, Lab Chip 12 (2012) 515–545. https://doi.org/10.1039/C2LC20799K.
[60] Characterization of syringe-pump-driven versus pressure-driven microfluidic flows | IEEE Conference Publication | IEEE Xplore, (n.d.). https://ieeexplore.ieee.org/document/7337207 (accessed July 11, 2023).
[61] M. Dilla, A. E. Becerikli, A. Jakubowski, R. Schlögl, S. Ristig, Development of a tubular continuous flow reactor for the investigation of improved gas–solid interaction in photocatalytic CO 2 reduction on TiO 2, Photochemical & Photobiological Sciences 18 (2019) 314–318. https://doi.org/10.1039/C8PP00518D.
[62] Fittings 101 Guide, IDEX Health & Science (n.d.). https://www.idex-hs.com/resources/resources-detail/fittings-101-guide (accessed July 13, 2023).

[63] S. Takeuchi, P. Garstecki, D.B. Weibel, G.M. Whitesides, An Axisymmetric Flow-Focusing Microfluidic Device, Advanced Materials 17 (2005) 1067–1072. https://doi.org/10.1002/adma.200401738.
[64] A.M. Gañán-Calvo, J.M. Montanero, L. Martín-Banderas, M. Flores-Mosquera, Building functional materials for health care and pharmacy from microfluidic principles and Flow Focusing, Advanced Drug Delivery Reviews 65 (2013) 1447–1469. https://doi.org/10.1016/j.addr.2013.08.003.
[65] A. B. Lowe, Thiol-ene "click" reactions and recent applications in polymer and materials synthesis, Polymer Chemistry 1 (2010) 17–36. https://doi.org/10.1039/B9PY00216B.
[66] A. Otte, F. Sharifi, K. Park, Interfacial tension effects on the properties of PLGA microparticles, Colloids and Surfaces B: Biointerfaces 196 (2020) 111300. https://doi.org/10.1016/j.colsurfb.2020.111300.
[67] S.E. Gilchrist, D.L. Rickard, K. Letchford, D. Needham, H.M. Burt, Phase Separation Behavior of Fusidic Acid and Rifampicin in PLGA Microspheres, Mol. Pharmaceutics 9 (2012) 1489–1501. https://doi.org/10.1021/mp300099f.
[68] H. Katou, A.J. Wandrey, B. Gander, Kinetics of solvent extraction/evaporation process for PLGA microparticle fabrication, International Journal of Pharmaceutics 364 (2008) 45–53. https://doi.org/10.1016/j.ijpharm.2008.08.015.
[69] M.M. Arnold, E.M. Gorman, L.J. Schieber, E.J. Munson, C. Berkland, NanoCipro encapsulation in monodisperse large porous PLGA microparticles, Journal of Controlled Release 121 (2007) 100–109. https://doi.org/10.1016/j.jconrel.2007.05.039.
[70] M.A. Sharaf, J.E. Mark, The Effects of Cross-Linking and Strain on the Glass Transition Temperature of a Polymer Network, Rubber Chemistry and Technology 53 (1980) 982–987. https://doi.org/10.5254/1.3535073.
[71] S.C. George, M. knörgen, S. Thomas, Effect of nature and extent of crosslinking on swelling and mechanical behavior of styrene–butadiene rubber membranes, Journal of Membrane Science 163 (1999) 1–17. https://doi.org/10.1016/S0376-7388(99)00098-8.
[72] F. Le Devedec, H. Boucher, D. Dubins, C. Allen, Factors Controlling Drug Release in Cross-linked Poly(valerolactone) Based Matrices, Mol. Pharmaceutics 15 (2018) 1565–1577. https://doi.org/10.1021/acs.molpharmaceut.7b01102.
[73] J.L. Valentín, J. Carretero-González, I. Mora-Barrantes, W. Chassé, K. Saalwächter, Uncertainties in the Determination of Cross-Link Density by Equilibrium Swelling Experiments in Natural Rubber, Macromolecules 41 (2008) 4717–4729. https://doi.org/10.1021/ma8005087.
[74] A.R. Tellegen, I. Rudnik-Jansen, L. Utomo, S. Versteeg, M. Beukers, R. Maarschalkerweerd, D. van Zuilen, N.J. van Klaveren, K. Houben, E. Teske, P.R. van Weeren, N. Karssemakers-Degen, G. Mihov, J. Thies, N. Eijkelkamp, L.B. Creemers, B.P. Meij, M.A. Tryfonidou, Sustained release of locally delivered celecoxib provides pain relief for osteoarthritis: a proof of concept in dog patients, Osteoarthritis and Cartilage 31 (2023) 351–362. https://doi.org/10.1016/j.joca.2022.11.008.
[75] H. Tsuji, Poly(lactide) Stereocomplexes: Formation, Structure, Properties, Degradation, and Applications, Macromolecular Bioscience 5 (2005) 569–597. https://doi.org/10.1002/mabi.200500062.
[76] N.M. Shah, M.D. Pool, A.T. Metters, Influence of Network Structure on the Degradation of Photo-Cross-Linked PLA-b-PEG-b-PLA Hydrogels, Biomacromolecules 7 (2006) 3171–3177. https://doi.org/10.1021/bm060339z.
[77] M.N. Mason, A.T. Metters, C.N. Bowman, K.S. Anseth, Predicting Controlled-Release Behavior of Degradable PLA-b-PEG-b-PLA Hydrogels, Macromolecules 34 (2001) 4630–4635. https://doi.org/10.1021/ma010025y.
[78] K.S. Anseth, A.T. Metters, S.J. Bryant, P.J. Martens, J.H. Elisseeff, C.N. Bowman, In situ forming degradable networks and their application in tissue engineering and drug delivery, Journal of Controlled Release 78 (2002) 199–209. https://doi.org/10.1016/S0168-3659(01)00500-4.
[79] A.R. Tellegen, I. Rudnik-Jansen, B. Pouran, H.M. de Visser, H.H. Weinans, R.E. Thomas, M.J.L. Kik, G.C.M. Grinwis, J.C. Thies, N. Woike, G. Mihov, P.J. Emans, B.P. Meij, L.B. Creemers, M.A. Tryfonidou, Controlled release of celecoxib inhibits inflammation, bone cysts and osteophyte formation in a preclinical model of osteoarthritis, Drug Delivery 25 (2018) 1438–1447. https://doi.org/10.1080/10717544.2018.1482971.
[80] M.-C. Villa-Hermosilla, S. Negro, E. Barcia, C. Hurtado, C. Montejo, M. Alonso, A. Fernandez-Carballido, Celecoxib Microparticles for Inhalation in COVID-19-Related Acute Respiratory Distress Syndrome, Pharmaceutics 14 (2022) 1392. https://doi.org/10.3390/pharmaceutics14071392.
[81] M. Homar, N. Ubrich, F.E. Ghazouani, J. Kristl, J. Kerč, P. Maincent, Influence of polymers on the bioavailability of microencapsulated celecoxib, Journal of Microencapsulation 24 (2007) 621–633. https://doi.org/10.1080/09637480701497360.
[82] D. Grizić, A. Lamprecht, Predictability of drug encapsulation and release from propylene carbonate/PLGA microparticles, International Journal of Pharmaceutics 586 (2020) 119601. https://doi.org/10.1016/j.ijpharm.2020.119601.

[83] A.C. Amrite, S.P. Ayalasomayajula, N.P.S. Cheruvu, U.B. Kompella, Single Periocular Injection of Celecoxib-PLGA Microparticles Inhibits Diabetes-Induced Elevations in Retinal PGE2, VEGF, and Vascular Leakage, Investigative Ophthalmology & Visual Science 47 (2006) 1149–1160. https://doi.org/10.1167/iovs.05-0531.
[84] S.P. Ayalasomayajula, U.B. Kompella, Subconjunctivally administered celecoxib-PLGA microparticles sustain retinal drug levels and alleviate diabetes-induced oxidative stress in a rat model, European Journal of Pharmacology 511 (2005) 191–198. https://doi.org/10.1016/j.ejphar.2005.02.019.
[85] F. Wan, A. Bohr, M.J. Maltesen, S. Bjerregaard, C. Foged, J. Rantanen, M. Yang, Critical Solvent Properties Affecting the Particle Formation Process and Characteristics of Celecoxib-Loaded PLGA Microparticles via Spray-Drying, Pharm Res 30 (2013) 1065–1076. https://doi.org/10.1007/s11095-012-0943-x.
[86] C. Salgado, L. Guénée, R. Černý, E. Allémann, O. Jordan, Nano wet milled celecoxib extended release microparticles for local management of chronic inflammation, International Journal of Pharmaceutics 589 (2020) 119783. https://doi.org/10.1016/j.ijpharm.2020.119783.
[87] A. Bohr, F. Wan, J. Kristensen, M. Dyas, E. Stride, S. Baldursdottír, M. Edirisinghe, M. Yang, Pharmaceutical microparticle engineering with electrospraying: the role of mixed solvent systems in particle formation and characteristics, J Mater Sci: Mater Med 26 (2015) 61. https://doi.org/10.1007/s10856-015-5379-5.
[88] A. Bohr, J. Kristensen, M. Dyas, M. Edirisinghe, E. Stride, Release profile and characteristics of electrosprayed particles for oral delivery of a practically insoluble drug, Journal of The Royal Society Interface 9 (2012) 2437–2449. https://doi.org/10.1098/rsif.2012.0166.